Hari, V., Villarini, G., Zhang, W. (2020):
Fidelity of global climate models in representing the horizontal water vapour transport
Int. J. Climatol. **40** (13), 5714 – 5726

https://doi.org/10.1002/joc.6546

Fidelity of Global Climate Models in Representing the Horizontal Water Vapor Transport

Vittal H.[1,2], Gabriele Villarini[1], and Wei Zhang[1]

[1.] IIHR-Hydroscience & Engineering, The University of Iowa, Iowa City, Iowa, USA

[2.]Department of Computational Hydrosystems, Helmholtz Centre for Environmental Research, UFZ, Leipzig, Germany

Corresponding author: Vittal H., email: vittalhari@uiowa.edu

Submitted to International Journal of Climatology

Abstract

The horizontal water vapor transport (IVT) is one of the key variables connected to precipitation extremes and floods, especially in the mid-latitudinal countries, and represents a key link between water sources and sink regions. Because of its significant impacts, great efforts have been made to examine IVT and its projected changes in response to changes to the climate system, leveraging outputs from global climate models (GCMs). However, to gain more confidence in the projections, it is important to evaluate how well the GCMs can reproduce the historical past.

Here, we assess how well ten GCMs archived in the Climate Model Intercomparison Project Phase 5 can reproduce the spatial and temporal patterns of the mean and 85th percentile of the IVT distribution. Analyses are performed at the global scale using outputs at the six-hourly resolution, and four different reanalysis products as reference. We find that the results from the GCMs are in good agreement with the reanalyses in terms of the IVT climatology; however, the GCMs fail to capture the trends in IVT, with almost all the models showing a negative correlation with the reanalysis data for both the mean and the 85th percentile. We also extend our analyses to the daily time scale, reaching the same conclusions drawn for the six-hourly resolution. These results further highlight the need for a careful evaluation of the GCM outputs in reproducing the observed IVT distribution.

1. Introduction

Water vapor is one of the most important variables in terms of climate feedback because of moist dynamics and radiative heating effects, and thus plays a crucial role in the earth's climate system (e.g., Trenberth et al., 2005). Trenberth and Stepaniak (2003) argued that, irrespective of the weather system, water vapor serves as the primary source for precipitation across the globe, mainly by influencing the tropospheric diabatic heating structure and thereby adding latent heat to the system. As the climate warms, the water vapor in the atmosphere increases at a rate faster than the total precipitation amount (Vittal et al., 2016). Studies based on both observations and numerical simulations (e.g., Allen and Ingram, 2002; Kharin et al., 2007) estimated that the water vapor content in the atmosphere increases at a rate of 7%/K following the Clausius-Clapeyron relationship, primarily driven by the surface heat budget (e.g., Trenberth et al., 2003). This process results in changes in the dynamics of the precipitation characteristics by modifying its intensity, frequency and duration. Further, different studies have attributed significant increases in precipitation extremes to the abundant availability of water vapor in a warmer atmosphere (e.g., Allen and Ingram, 2002; Held and Soden, 2006; Muller et al., 2011). These changes in precipitation patterns ultimately lead to the observed severity of floods and droughts, and all the societal and economic impacts associated with these natural hazards. Thus, efforts towards improving our understanding of the dynamics of water vapor under warming conditions can provide information critical for our mitigation and adaptation strategies.

In addition to precipitation, water vapor and its transport are key ingredients for atmospheric rivers (ARs). These events play a crucial role in the meridional water vapor transport from the tropics to the midlatitudes (Zhu and Newell, 1998; Gimeno et al., 2014) and are usually characterized by high moisture content together with a strong low-level jet (e.g., Ralph et al., 2004). ARs are often associated with heavy precipitation when they make landfall due to orographic lifting, especially in mid-latitude coastal regions such as the western United States, western Europe, and South America (e.g., Guan and Waliser 2015; Waliser and Guan 2015; Lavers and Villarini 2015; Espinoza et al., 2018). Although Dettinger (2013) reported that ARs play a significant role in alleviating the drought condition in the western United States, they are also responsible for severe riverine and coastal flooding (e.g., Barth et al. 2017; Khouakhi and Villarini, 2016; Lavers et al., 2011), leading to devastating effects on the affected regions.

Given the importance the water vapor has towards socio-economic welfare, different studies examined the changes in its characteristics in warming scenarios in terms of integrated water vapor transport (IVT), the key link between source and sink regions of moisture (Lavers et al., 2015), and ARs (characterized by the percentile rank of IVT). For example, Lavers et al. (2015) investigated the projected changes in IVT at the daily scale using 22 global circulation models (GCMs) for two emission scenarios. They found that in the more extreme emission scenario, the multimodal IVT mean increases by 30-40%, especially in the North Pacific and Atlantic regions due mainly to the availability of higher atmospheric water vapor content. Dettinger (2011) focused on the landfalling ARs in California using the outputs archived in the Coupled Model

Intercomparison Project Phase 3 (CMIP3) models and found an increase in the frequency of ARs of ~ 30% at the end of the 21st century. Warner et al. (2015) extended the work of Dettinger (2011) focusing on models from the Fifth Coupled Model Intercomparison Project (CMIP5) and the west coast of North America; they found a significant increase in the IVT extreme values and in the AR days of about 300%. Lavers et al. (2013) and Gao et al. (2016) also showed an increase in IVT and AR frequencies using CMIP5 models across western Europe. Among others, the climate model outputs were also extensively used by Pierce et al., (2013), Gao et al. (2015), Lavers et al. (2013) Shields and Kiehl (2016) and Ramos et al. (2016), showing an increase in IVT under future scenarios for regions such as the coast of California, Western Europe and North Atlantic.

Understanding the behavior of water vapor transport in a changing climate represents one of the critical challenges in climate studies, as highlighted by numerous studies that address this issue (e.g., Creese and Washington, 2018; Tamoffo et al, 2019). It is also clear that the GCMs have indeed been playing a pivotal role in understanding the future changes in water vapor transport. However, given the existence of inherent uncertainties in the GCM outputs (e.g., Randall et al., 2007), it is of the utmost importance to provide insights into the credibility of these models in simulating the historical spatio-temporal variations of IVT before moving forward with an assessment of their projected changes. There are limited observation/reanalysis-based studies related to the evaluation of integrated water vapor. Trenberth et al. (2005) compared two different reanalysis products to satellite-based dataset and found that the reanalysis products can overall capture the spatial and temporal patterns of water vapor. However, much less is known about how well GCMs can reproduce the spatial and temporal patterns of IVT, especially at the sub-daily scale. Therefore, this study aims to comprehensively evaluate the spatial pattern and seasonal variations of IVT at the six-hourly and daily scales by leveraging multiple reanalysis products and CMIP5 outputs (Historical and Atmospheric Model Intercomparison Project (AMIP) simulations). We also examine how well the CMIP5 models can reproduce the temporal trends in different reanalyses data. These analyses will highlight the strength and weakness of the CMIP5 models, providing valuable insights towards the interpretation of projected changes in IVT.

2. Data and Methods

We use the water vapor transport from four atmospheric reanalysis data sets as references for the evaluation of the GCMs: 1) National Centers for Environmental Prediction (NCEP)/National Center for Atmospheric Research (NCAR) reanalysis project (NCEP-NCAR) (Kalnay et al., 1996); 2) the Japan Meteorological Agency (JMA)'s Japanese 55 year Reanalysis (JRA-55) (Kobayashi et al., 2015); 3) European Centre for Medium-Range Weather Forecasts (ECMWF) reanalysis project (ERA-Interim) (Dee et al., 2011); 4) the National Aeronautics and Space Administration (NASA)'s Modern-Era Retrospective analysis for Research and Applications, version 2 (MERRA2) (Gelaro et al., 2017). All of the reanalyses have six-hour temporal resolution. In terms of climate models, we consider 15 CMIP5 models (10 historical and 5 AMIP simulations) with six-hourly outputs, as summarized in Table 1.

To calculate the magnitude of IVT, we use specific humidity, and the meridional and zonal wind components from the surface (~1000 hPa) to 300 hPa pressure levels (e.g., Zhu and Newell, 1998; Neiman et al., 2008; Lavers et al., 2012):

$$IVT\ (kg\ m^{-1}\ s^{-1}) = \sqrt{\left(\frac{1}{g}\int_{1000}^{300} qu dp\right)^2 + \left(\frac{1}{g}\int_{1000}^{300} qv dp\right)^2} \quad (1)$$

where q is the specific humidity (kg/kg), u and v are the zonal and meridional wind components (m/s) respectively, g is the acceleration due to gravity (m/s^2) and dp is the pressure level difference. We compare the spatio-temporal pattern of the mean and 85th percentile (i.e., used for the identification of ARs) of the IVT for four different seasons (DJF: December-January-February; MAM: March-April-May; JJA: June-July-August; SON: September-October-November). For comparison purpose, we interpolate the reference reanalysis data to the respective GCMs/reanalysis resolutions.

We evaluate the climatology and trends of IVT simulated by the climate models. We use the nonparametric Mann-Kendall test (Kendall, 1975) for estimating trends. Further, we use Taylor's diagram (Taylor, 2001) to compare reanalysis and climate model simulations in representing the climatology and trends of IVT. The advantage of Taylor's diagram is that it can graphically compare correlation, standard deviation, and the root mean square errors (RMSE) of the datasets in one single diagram.

3. Results and Discussion

We start by evaluating the seasonal climatology of IVT based on the reanalyses data in terms of its mean and 85th percentile. Figure 1 shows the comparison of the climatology of mean IVT for the four reanalysis products from 1979-2015. For comparison purpose, we considered MERRA2 as the reference data in this case. Although each reanalysis data set is developed with distinct models, physical processes, and resolutions, all of them assimilate various radiosonde observations and satellite products using different assimilation techniques. We note that the radiance data from Atmospheric Infrared Sounder (AIRS), Advanced Microwave Sounding Unit (AMSU), or both is assimilated in MERRA2 (Gelaro et al., 2017). Because of this reason, Jiang et al. (2019) could notice that the spatio-temporal patterns of precipitable water vapor from MERRA2 along with ERA-Interim product is able to follow the observations very closely. Therefore, we select MERRA2 as the reference to compare other reanalysis products in our study. The present study also compares the reanalysis products in simulating the IVT for different seasons, because there are regions that exhibit a strong seasonality in terms of precipitation. For example, The U.S. West Coast receives the majority of its precipitation during the winter months (Warner et al. 2008), with the most extreme events that are driven by atmospheric rivers [ARs] (Ralph et al. 2005, 2006; Dettinger 2011; Warner et al. 2015). In European countries, the predominant links between precipitation extremes and ARs are found in SON and DJF, with many regions having more than 40% of precipitation extremes caused by ARs (Lavers and Villarini, 2013). On the other hand, in the south Asian monsoon regions, the AR frequency largely occurs during DJF, JJA and SON, and it also drives precipitation extremes over these regions (Thapa et al., 2018). Depending on the seasons, the IVT storm track is prominently evident in the North Pacific and Atlantic regions. The poleward migration of the extratropical IVT storm track during the winter and summer seasons is also apparent. There is a region with high values of IVT along the East Asian coast during JJA, which is likely associated with tropical cyclone activity (Lavers et al., 2015). The mean fields also captured the high magnitude of IVT during the Indian monsoon region in JJA. Overall, the spatial pattern of IVT is quite similar to Lavers et al. (2015), even though our focus is on the six-hourly scale compared to their analyses performed at the daily scale. The right panels of Figure 1 show the comparisons of the reanalysis datasets, highlighting the capability of reanalyses data in capturing the spatial pattern of mean IVT, with high correlation and small RMSE values compared with MERRA2.

The midlatitude extratropical cyclones and ARs are usually associated with the high magnitude of IVT (Lavers et al., 2015), which is responsible for extreme precipitation and flooding. Here we focus on the 85th percentile of the IVT distribution because it has been used to identify ARs (Figure 2; e.g., Lavers et al., 2012). Overall, the spatial patterns of the 85th percentile of the IVT distribution are similar to what found for the mean IVT (Figure 1). As with the mean fields, all the reanalysis products could represent the patterns of the 85th percentile of IVT (Figure 2, right panels). These findings are consistent with other studies (e.g., Lavers et al. 2015), and we would expect similar spatial patterns between mean and 85th percentile, with higher IVT values associated with the latter one.

Up to this point, we have compared the results by the four reanalysis products in reproducing the spatial patterns of seasonal IVT, and found that they all provide similar answers, with NCEP/NCAR that slightly underperforms comparted to the other ones. NCEP/NCAR reanalysis uses neither AIRS nor AMSU (Jiang et al., 2019), leading to a relatively lower performance among the reanalysis data product used in the study. Now we move to the examination of how well the GCMs can reproduce the results by the reanalyses (Figure 3), using JRA-55. It is already shown from our analysis that both MERRA2 and JRA55 (Figure 1 and 2) had no significant differences in representing both spatio-temporal variation of IVT. The added advantage of JRA-55 dataset is that it covers a longer period and this is the reason we went with JRA-55 for further analysis. Overall, the models capture both the intensity and pattern of IVT quite well, as shown from the Taylor's diagram (Figure 3) for all the seasons. Most of the models show a high correlation with the JRA55's mean IVT, along with smaller RMSE values and a similar standard deviation. We also performed similar analyses by considering the 85th percentile of the IVT distribution (Figure 4); the models can capture the spatial pattern and intensity of IVT very well, similar to what observed for the mean IVT.

The findings from our analyses at the 6-hourly scale are comparable to those at the daily scale by Lavers et al. (2015), which compared the multimodel historical mean obtained from 22 climate models with respect to ERA-Interim. However, they found some discrepancies, especially during JJA, with high IVT values particularly over the eastern equatorial Pacific region. This is consistent with Dai (2006), who highlighted the difficulties by most models in reproducing various climatic parameters over the eastern equatorial Pacific region. Despite these issues, the overall performance of the GCMs in capturing the climatology of the mean and 85th percentile of the IVT is generally very satisfactory.

Although there is evidence that the GCMs are capable of capturing the climatology of IVT, whether these models are able to capture the overall trends in this quantity has received little attention in the literature. Given that we are working with the historical run and not the AMIP simulations, we would not expect the models to reproduce the year-to-year IVT values; however, it is reasonable to expect the models to be able to reproduce the overall trends in the reanalyses, and this is what we consider here. First, we estimate the patterns in IVT both for the mean and 85th percentile using the non-parametric Mann-Kendall test. Figure 5 shows the long-term trends in the seasonal mean IVT from 1958 to 2005 based on JRA55. Based on these results, there is a significant increase in the average IVT in the equatorial Atlantic region and a decrease in the Northern Indian Ocean region for each of the four seasons; there is also an increasing trend in the southern equatorial region (0º to 30º S). The same conclusions are valid for the 85th percentile of the IVT distribution (Figure 6), similar to the responses of extreme precipitation to increased CO_2 concentration (Pfahl et al. 2017; Zhang et al. 2017). Supplementary Figures S1 and S2 show the comparison of the trend analysis for mean and 85th percentile of IVT for all the reanalyses for the common 1979-2015 period. The spatial patterns of the trends for the shorter period are similar to the longer one (compare the JRA55 results in Supplementary Figures S1-S2 and those in Figures 5-6). Among the different reanalysis products, NCEP-NCAR is the one that tends to underperform with respect to the other ones, especially in the tropical regions.

In addition to comparing the different reanalysis products, we now focus on the GCMs, summarizing their spatial patterns of the trends from 1958-2005 for the different seasons (Figure 7 and 8, and Supplementary Figures S3-S10). Based on these results (Supplementary Figures S3-S6), it is clear that, irrespective of seasons, the patterns of the trends in the GCMs do not match what we found using JRA55. More specifically, there are diametric opposite trends in some regions, especially in the tropics. We observe similar patterns for the 85th percentile (Supplementary Figures S7-S10). These visual assessments are further substantiated by the Taylor's diagram for the mean (Figure 7) and 85th percentile (Figure 8). Overall, the ten GCMs considered here were not able to satisfactorily capture the trend patterns, as documented by their low values of correlation coefficient and large RMSE; this statement is valid regardless of the season.

To examine whether these results can be rectified when using sea surface temperature and sea ice as boundary conditions, we also compare the performance of the AMIP simulations and reanalyses along with the models over the 1980-2005 period. In terms of spatial climatological patterns, there is a close agreement with the IVT from reanalyses, regardless of model, IVT quantity and season, with the AMIP runs that tend to perform better than the corresponding historical runs (Figures 3-4.) This good performance, however, does not transfer to the trends in IVT (Figures 7-8): the results from the AMIP runs do not improve over the historical simulations, indicating that there is still room for improvement in terms of the representation of the trends in IVT. With that said, it is worth highlighting that the tight agreement among reanalysis products in terms of spatial variability in IVT is not present in the trend results, pointing to the difficulties in reproducing its temporal variability even when observations are assimilated. A potential reason behind the limited capability of the GCMs in representing IVT trends may be due to their difficulties in capturing the dynamics of variables such as specific humidity, u and v components of winds. Supplementary Figures S11 and S12 show the climatology and trends in QU (i.e., vertically integrated specific humidity and u-wind component from the surface to the troposphere) and QV (i.e., vertically integrated specific humidity and v-wind component from surface to troposphere). Based on these results, the models can reproduce the climatology of QU and QV, but fail to capture the spatial patterns of trends, leading to the abovementioned issues in the representation of IVT trends from climate models.

As mentioned before, all the analyses are based on the six-hourly data. We have also examined how the results would change if we focused on the daily temporal resolution (Supplementary Figure S13). Though we notice a slight change in the values of the correlation coefficient, standard deviation, and RMSE, the overall results support the conclusions that were drawn with the data at the six-hourly temporal resolution.

4. Conclusions

The transport of water vapor represents the key ingredient in the identification of atmospheric rivers, which are phenomena that can cause extreme precipitation and flooding across large areas of the midlatitudes. As the climate warms, the availability of the water vapor is projected to increase, leading to an intensification of the atmospheric transport of moisture across the midlatitudes. Numerous studies linked the increased atmospheric transport of moisture to the flooding in regions such as western North America, South America, and Western Europe. Thus, it is of high importance to better understand current and future changes in this quantity to better mitigate and adapt to these extreme events.

The goal of this study was to evaluate the performance of ten GCMs from CMIP5 in reproducing the historical spatial and temporal variability in IVT quantities (i.e., mean and 85^{th}

percentile of the distribution) at the seasonal scale and across the globe. Our main findings can be summarized as follows:

- We showed that the reanalysis and climate model outputs can capture very well the climatology of the IVT in terms of both mean and 85th percentile. This statement is valid regardless of the seasons and GCM experiments (i.e., historical and AMIP).
- The good performance in reproducing the spatial patterns of IVT does not transfer to the analyses of its temporal variability. The GCMs show trend patterns that are very different from those by JRA55, regardless of the IVT quantity. This may be due to inability of the climate models in reproducing the trends in individual components, viz., specific humidity, zonal and meridional winds.
- To examine the potential role of boundary conditions in explaining these findings, we analyzed the AMIP runs. Our results do not point to an improved performance when sea surface temperature and sea ice are provided as boundary conditions.
- While the GCMs are not able to capture the trends in IVT, it is worth highlighting the difficulties by the reanalysis products as well. These findings suggest that capturing the trends in IVT still represents a significant challenge from a modeling perspective.
- These statements are valid both at the six-hourly and daily time scales.

Here we have focused on analyses at the global scale. However, future studies could focus on analyses at a more regional scale, with particular emphasis on those areas where IVT plays an important role in causing extreme precipitation. As shown by Espinoza et al. (2018), there are discrepancies in the changes in AR frequency across different regions, with some models projecting a decreasing trend in the subtropical Pacific regions near western Pacific and North America. These disagreements may be due to shifts in storm tracks or subtropical jet streams (e.g., Hagos et al., 2016; Shields and Kiehl, 2016; Zhang and Villarini, 2018), which could not be well captured by the models. This issue has also been discussed by Gao et al. (2016), who highlighted the uncertainties in the projections of ARs along western North America and Western Europe, warranting more in-depth understanding of the dynamics in these regions.

Acknowledgements: Vittal H. acknowledges the support by Fulbright-Kalam Fellowship (Grant 2338/FKPDR/2018). This study was also supported by the National Science Foundation under CAREER Grant AGS-1349827 and the USACE Institute for Water Resources.

Supporting information

This section describes the supporting information regarding: grid-wise trend analysis of mean and 85th percentile IVT from 1979-2015 for the four different reanalysis products considered in the study. Further, it also contains the IVT trends in mean and 85th percentile for the climate models for different seasons. Finally, it contains the comparison of 6 hourly and daily IVT fields.

References

Allen, M.R. and Ingram, W.J., 2002. Constraints on future changes in climate and the hydrologic cycle. Nature, 419(6903): 228.

Barth, N.A., Villarini, G., Nayak, M.A. and White, K., 2017. Mixed populations and annual flood frequency estimates in the western United States: The role of atmospheric rivers. Water Resources Research, 53(1): 257-269.

Creese, A., and Washington, R. 2018. A process-based assessment of CMIP5 rainfall in the Congo Basin: the September–November rainy season. Journal of Climate, 31(18), 7417-7439.

Dai, A., 2006. Precipitation characteristics in eighteen coupled climate models. Journal of Climate, 19(18): 4605-4630.

Dee, D.P., Uppala, S.M., Simmons, A.J., Berrisford, P., Poli, P., Kobayashi, S., Andrae, U., Balmaseda, M.A., Balsamo, G., Bauer, D.P. and Bechtold, P., 2011. The ERA-Interim reanalysis: Configuration and performance of the data assimilation system. Quarterly Journal of the royal meteorological society, 137(656): 553-597.

Dettinger, M., 2011. Climate change, atmospheric rivers, and floods in California–a multimodel analysis of storm frequency and magnitude changes 1. JAWRA Journal of the American Water Resources Association, 47(3): 514-523.

Dettinger, M.D., 2013. Atmospheric rivers as drought busters on the US West Coast. Journal of Hydrometeorology, 14(6): 1721-1732.

Espinoza, V., Waliser, D.E., Guan, B., Lavers, D.A. and Ralph, F.M., 2018. Global analysis of climate change projection effects on atmospheric rivers. Geophysical Research Letters, 45(9): 4299-4308.

Gao, Y., Lu, J. and Leung, L.R., 2016. Uncertainties in projecting future changes in atmospheric rivers and their impacts on heavy precipitation over Europe. Journal of Climate, 29(18): 6711-6726.

Gao, Y., Lu, J., Leung, L.R., Yang, Q., Hagos, S. and Qian, Y., 2015. Dynamical and thermodynamical modulations on future changes of landfalling atmospheric rivers over western North America. Geophysical Research Letters, 42(17): 7179-7186.

Gelaro, R., McCarty, W., Suárez, M.J., Todling, R., Molod, A., Takacs, L., Randles, C.A., Darmenov, A., Bosilovich, M.G., Reichle, R. and Wargan, K., 2017. The modern-era retrospective analysis for research and applications, version 2 (MERRA-2). Journal of Climate, 30(14): 5419-5454.

Gimeno, L., Nieto, R., Vázquez, M. and Lavers, D.A., 2014. Atmospheric rivers: A mini-review. Frontiers in Earth Science, 2:.2.

Guan, B. and Waliser, D.E., 2015. Detection of atmospheric rivers: Evaluation and application of an algorithm for global studies. Journal of Geophysical Research: Atmospheres, 120(24): 12514-12535.

Hagos, S.M., Leung, L.R., Yoon, J.H., Lu, J. and Gao, Y., 2016. A projection of changes in landfalling atmospheric river frequency and extreme precipitation over western North America from the Large Ensemble CESM simulations. Geophysical Research Letters, 43(3): 1357-1363.

Held, I.M. and Soden, B.J., 2006. Robust responses of the hydrological cycle to global warming. Journal of climate, 19(21):.5686-5699.

Jiang, J., Zhou, T. and Zhang, W., 2019. Evaluation of satellite and reanalysis precipitable water vapor datasets against radiosonde observations in Central Asia. Earth and Space Science, doi: https://doi.org/10.1029/2019EA000654.

Kalnay, E., Kanamitsu, M., Kistler, R., Collins, W., Deaven, D., Gandin, L., Iredell, M., Saha, S., White, G., Woollen, J. and Zhu, Y., 1996. The NCEP/NCAR 40-year reanalysis project. Bulletin of the American meteorological Society, 77(3): 437-472.

Kendall MG (1975) Rank Correlation Methods. Griffin, London

Kharin, V.V., Zwiers, F.W., Zhang, X. and Hegerl, G.C., 2007. Changes in temperature and precipitation extremes in the IPCC ensemble of global coupled model simulations. Journal of Climate, 20(8): 1419-1444.

Khouakhi, A., and G. Villarini, 2016. On the relationship between atmospheric rivers and high sea water levels along the U.S. West Coast. Geophysical Research Letters, 43:8815-8822.

Kobayashi, S., Ota, Y., Harada, Y., Ebita, A., Moriya, M., Onoda, H., Onogi, K., Kamahori, H., Kobayashi, C., Endo, H. and Miyaoka, K., 2015. The JRA-55 reanalysis: General specifications and basic characteristics. Journal of the Meteorological Society of Japan. Ser. II, 93(1): 5-48.

Lavers, D.A., Allan, R.P., Villarini, G., Lloyd-Hughes, B., Brayshaw, D.J. and Wade, A.J., 2013. Future changes in atmospheric rivers and their implications for winter flooding in Britain. Environmental Research Letters, 8(3): 034010.

Lavers, D.A., Allan, R.P., Wood, E.F., Villarini, G., Brayshaw, D.J. and Wade, A.J., 2011. Winter floods in Britain are connected to atmospheric rivers. Geophysical Research Letters, 38(23).

Lavers, D.A., Ralph, F.M., Waliser, D.E., Gershunov, A. and Dettinger, M.D., 2015. Climate change intensification of horizontal water vapor transport in CMIP5. Geophysical Research Letters, 42(13): 5617-5625.

Lavers, D.A. and Villarini, G., 2015. The contribution of atmospheric rivers to precipitation in Europe and the United States. Journal of Hydrology, 522: 382-390.

Lavers, D.A., Villarini, G., Allan, R.P., Wood, E.F. and Wade, A.J., 2012. The detection of atmospheric rivers in atmospheric reanalyses and their links to British winter floods and the large-scale climatic circulation. Journal of Geophysical Research: Atmospheres, 117(D20), doi:10.1029/2012JD018027

Muller, C.J., O'Gorman, P.A. and Back, L.E., 2011. Intensification of precipitation extremes with warming in a cloud-resolving model. Journal of Climate, 24(11): 2784-2800.

Neiman, P.J., Ralph, F.M., Wick, G.A., Kuo, Y.H., Wee, T.K., Ma, Z., Taylor, G.H. and Dettinger, M.D., 2008. Diagnosis of an intense atmospheric river impacting the Pacific Northwest: Storm summary and offshore vertical structure observed with COSMIC satellite retrievals. Monthly Weather Review, 136(11): 4398-4420.

Pfahl, S., O'Gorman, P.A. and Fischer, E.M., 2017. Understanding the regional pattern of projected future changes in extreme precipitation. Nature Climate Change, 7(6): 423.

Pierce, D.W., Cayan, D.R., Das, T., Maurer, E.P., Miller, N.L., Bao, Y., Kanamitsu, M., Yoshimura, K., Snyder, M.A., Sloan, L.C. and Franco, G., 2013. The key role of heavy precipitation events in climate model disagreements of future annual precipitation changes in California. Journal of Climate, 26(16): 5879-5896.

Ralph, F.M., Neiman, P.J. and Wick, G.A., 2004. Satellite and CALJET aircraft observations of atmospheric rivers over the eastern North Pacific Ocean during the winter of 1997/98. Monthly Weather Review, 132(7): 1721-1745.

Ralph, F. M., Neiman, P. J. and Rotunno, R., 2005. Dropsonde observations in low-level jets over the northeastern Pacific Ocean from CALJET-1998 and PACJET-2001: Mean vertical-profile and atmospheric-river characteristics. Monthly weather review, 133(4), 889-910.

Ralph, F. M., Neiman, P. J., Wick, G. A., Gutman, S. I., Dettinger, M. D., Cayan, D. R. and White, A. B. 2006. Flooding on California's Russian River: Role of atmospheric rivers. Geophysical Research Letters, 33(13).

Ramos, A. M., Tomé, R., Trigo, R. M., Liberato, M. L. and Pinto, J. G. 2016. Projected changes in atmospheric rivers affecting Europe in CMIP5 models. Geophysical Research Letters, 43(17), 9315-9323.

Randall DA, Wood RA, Bony S et al (2007) Climate Models and Their Evaluation. In: Climate Change 2007: The Physical Science Basis. Contribution of Working Group I to the Fourth Assessment Report of the Intergovernmental Panel on Climate Change, edited by: Solomon S, Qin D, Manning M, Chen Z, Marquis M, Averyt KB, Tignor M, Miller HL, Cambridge University Press, Cambridge, United Kingdom and New York, NY, USA.

Shields, C.A. and Kiehl, J.T., 2016. Atmospheric river landfall-latitude changes in future climate simulations. Geophysical Research Letters, 43(16): 8775-8782.

Tamoffo, A. T. et al., 2019. Process-oriented assessment of RCA4 regional climate model projections over the Congo Basin under 1.5°{C} and 2°{C} global warming levels: influence of regional moisture fluxes. Climate Dynamics, doi: https://doi.org/10.1007/s00382-019-04751-y

Taylor, K.E., 2001. Summarizing multiple aspects of model performance in a single diagram. Journal of Geophysical Research: Atmospheres, 106(D7): 7183-7192.

Thapa, K., Endreny, T. A. and Ferguson, C. R., 2018. Atmospheric rivers carry nonmonsoon extreme precipitation into Nepal. Journal of Geophysical Research: Atmospheres, 123(11), 5901-5912.

Trenberth, K.E., Dai, A., Rasmussen, R.M. and Parsons, D.B., 2003. The changing character of precipitation. Bulletin of the American Meteorological Society, 84(9): 1205-1218.

Trenberth, K.E., Fasullo, J. and Smith, L., 2005. Trends and variability in column-integrated atmospheric water vapor. Climate dynamics, 24(7-8): 741-758.

Trenberth, K.E. and Stepaniak, D.P., 2003. Covariability of components of poleward atmospheric energy transports on seasonal and interannual timescales. Journal of climate, 16(22): 3691-3705.

Vittal, H., Ghosh, S., Karmakar, S., Pathak, A., and Murtugudde, R. 2016. Lack of dependence of Indian summer monsoon rainfall extremes on temperature: an observational evidence. Scientific reports, 6, 31039.

Waliser, D. and Guan, B., 2017. Extreme winds and precipitation during landfall of atmospheric rivers. Nature Geoscience, 10(3): 179.

Warner, M.D., Mass, C.F. and Salathé Jr, E.P., 2015. Changes in winter atmospheric rivers along the North American west coast in CMIP5 climate models. Journal of Hydrometeorology, 16(1): 118-128.

Zhang, W., Villarini, G., Scoccimarro, E. and Vecchi, G.A., 2017. Stronger influences of increased CO2 on subdaily precipitation extremes than at the daily scale. Geophysical Research Letters, 44(14): 7464-7471.

Zhang, W. and Villarini, G., 2018. Uncovering the role of the East Asian jet stream and heterogeneities in atmospheric rivers affecting the western United States. Proceedings of the National Academy of Sciences, 115(5): 891-896.

Zhu, Y. and Newell, R. E., 1998. A proposed algorithm for moisture fluxes from atmospheric rivers. Monthly weather review, 126(3), 725-735.

Table 1: Details on the datasets used in this study

Model name	Institution	Runs	Horizontal resolution (latitude/longitude)
BNU-ESM	College of Global Change and Earth System Science, Beijing Normal University	Historical and AMIP	64×128
CanESM2	Canadian Centre for Climate Modelling and Analysis	Historical	64×128
CSIROMK3.6.0	CSIRO in collaboration with the Queensland Climate Change Centre of Excellence	Historical and AMIP	96×192
FGOALS-g2	LASG, Institute of Atmospheric Physics, Chinese Academy of Sciences; and CESS, Tsinghua University	Historical and AMIP	60×128
GFDL-CM3	Geophysical Fluid Dynamics Laboratory (GFDL)	Historical and AMIP	90×144
GFDL-ESM2G	GFDL	Historical	90×144
GFDL-ESM2M	GFDL	Historical	90×144
IPSL-CM5B-LR	Institut Pierre-Simon Laplace (IPSL)	Historical	96×96
IPSL-CM5A-LR	IPSL	Historical and AMIP	96×96
IPSL-CM5A-MR	IPSL	Historical	143×144
ERA-Interim	ECMWF	-	256×512
NCEP1	NCEP/NCAR	-	72 × 143
JRA55	JMA	-	148× 288
MERRA2	NASA GMAO	-	361 × 540


DJF
MAM
JJA
SON
60°N
30°N
0°
30°S
60°S
Standard Deviation
Correlation Coefficient
0.0
0.1
0.2
0.3
0.4
0.5
0.6
0.7
0.8
0.9
0.95
0.99
1.0
0
40
80
120
MERRA2
0.0
100.0
200.0
300.0
>400.0
IVT (kg/m-s)
+ JRA55
● ERA Interim
× NECP NCAR


DJF
MAM
JJA
SON
60° N
30° N
0°
30°S
60°S
Standard Deviation
Correlation Coefficient
0.0
0.1
0.2
0.3
0.4
0.5
0.6
0.7
0.8
0.9
0.95
0.99
1.0
0
50
100
150
45
90
135
180
MERRA2
0.0
200
400
>600
IVT (kg/m-s)
+ JRA55
● ERA Interim
× NECP NCAR

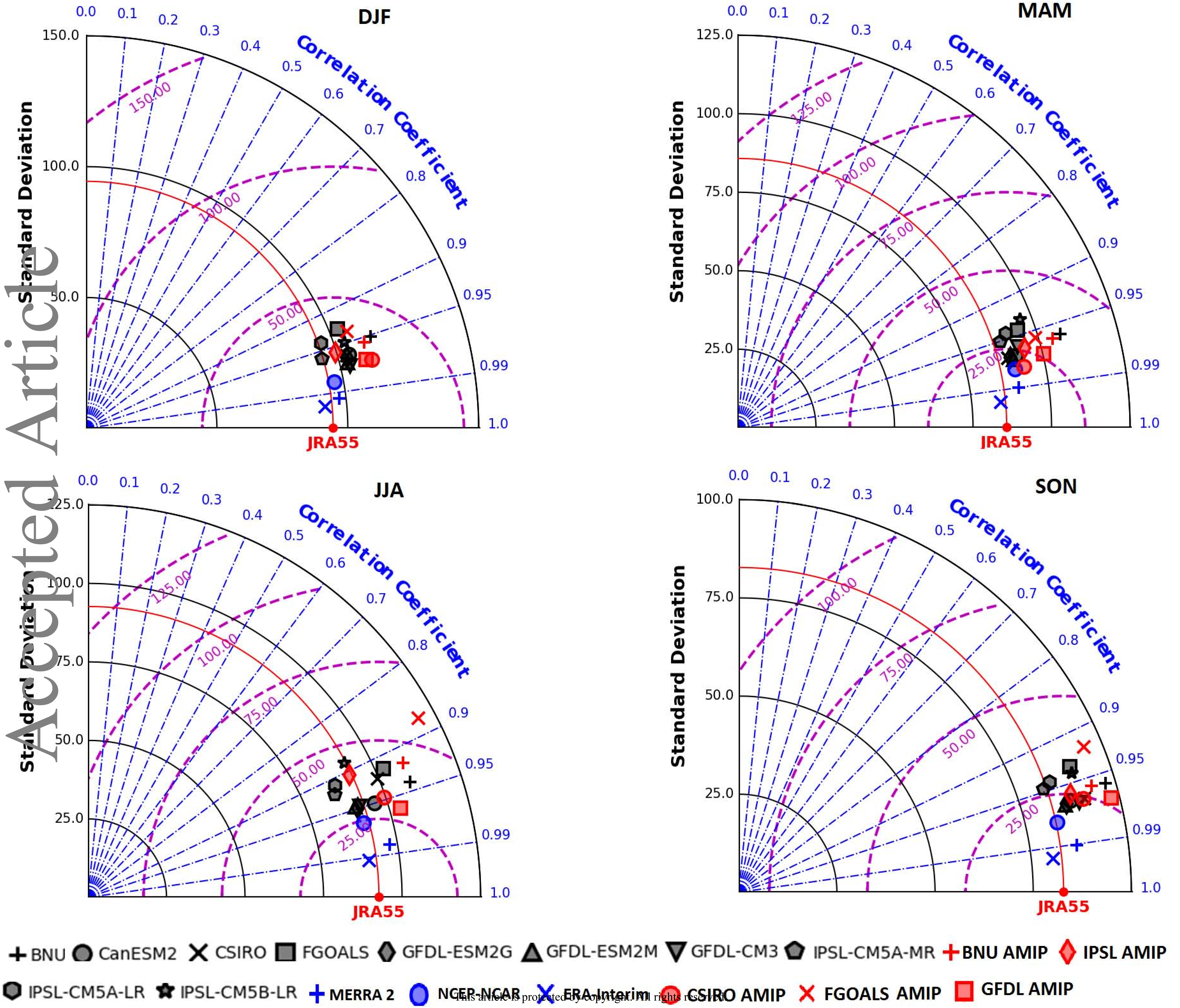
DJF
MAM
JJA
SON
Correlation Coefficient
Standard Deviation
JRA55
BNU
CanESM2
CSIRO
FGOALS
GFDL-ESM2G
GFDL-ESM2M
GFDL-CM3
IPSL-CM5A-MR
BNU AMIP
IPSL AMIP
IPSL-CM5A-LR
IPSL-CM5B-LR
MERRA 2
NCEP-NCAR
ERA-Interim
CSIRO AMIP
FGOALS AMIP
GFDL AMIP

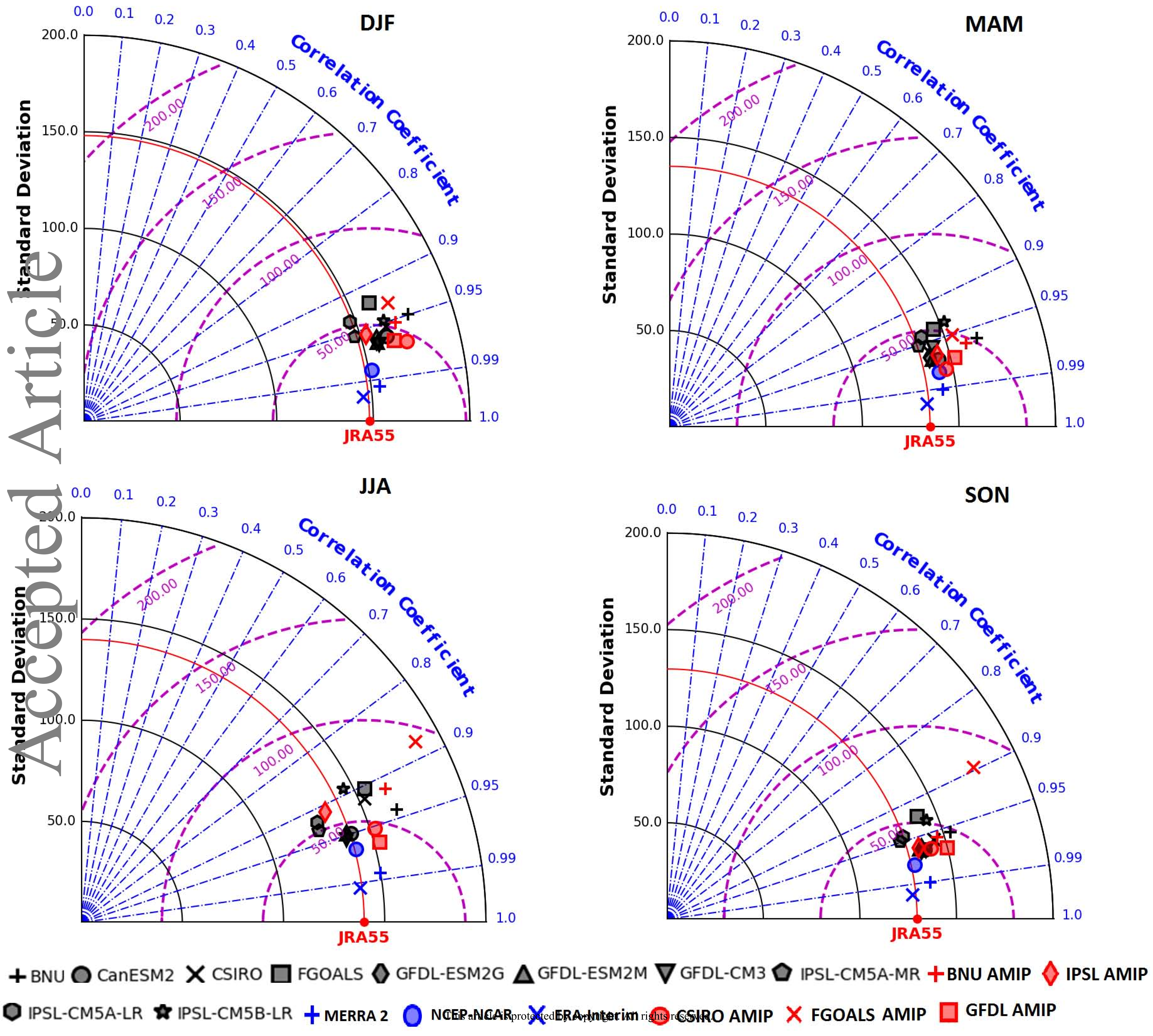
DJF
MAM
JJA
SON
Correlation Coefficient
Standard Deviation
JRA55
BNU
CanESM2
CSIRO
FGOALS
GFDL-ESM2G
GFDL-ESM2M
GFDL-CM3
IPSL-CM5A-MR
BNU AMIP
IPSL AMIP
IPSL-CM5A-LR
IPSL-CM5B-LR
MERRA 2
NCEP-NCAR
ERA-Interim
CSIRO AMIP
FGOALS AMIP
GFDL AMIP


DJF
MAM
JJA
SON
60°N
30°N
0°
30°S
60°S
-0.50
-0.25
0.00
0.25
0.50
Kendall's tau


DJF
MAM
JJA
SON
60°N
30°N
0°
30°S
60°S
-0.50
-0.25
0.00
0.25
0.50
Kendall's tau


Correlation Coefficient
DJF
MAM
JJA
SON
JRA55
Standard Deviation
BNU
CanESM2
CSIRO
FGOALS
GFDL-ESM2G
GFDL-ESM2M
GFDL-CM3
IPSL-CM5A-MR
BNU AMIP
IPSL AMIP
IPSL-CM5A-LR
IPSL-CM5B-LR
MERRA 2
NCEP-NCAR
ERA-Interim
CSIRO AMIP
FGOALS AMIP
GFDL AMIP


DJF
MAM
JJA
SON
Correlation Coefficient
Standard Deviation
JRA55
+ BNU ● CanESM2 ✕ CSIRO ■ FGOALS ◆ GFDL-ESM2G ▲ GFDL-ESM2M ▼ GFDL-CM3 ⬟ IPSL-CM5A-MR + BNU AMIP ◆ IPSL AMIP
⬢ IPSL-CM5A-LR ★ IPSL-CM5B-LR + MERRA 2 ● NCEP-NCAR ✕ ERA-Interim ● CSIRO AMIP ✕ FGOALS AMIP ■ GFDL AMIP